XMM-Newton CCF Release Note

XMM-CCF-REL-323

EPIC-pn Long-Term CTI and Energy Scale

M.J.S. Smith, M. Stuhlinger, R.D. Saxton, M.J. Freyberg

December 9, 2014

1 CCF Components

Name of CCF	VALDATE	EVALDATE	Blocks Changed	CAL Version	XSCS Flag
EPN_CTI_0045.CCF	2000-01-01T00:00:00		LONG_TERM_CTI NDSCLIN_GAIN COMB_EVT_OFFSET	3.232	NO

2 Changes

Here we present the following changes to the PN energy scale calibration introduced with SAS 14.0 and EPN_CTI_0045.CCF:

- An energy dependent long-term CTI (LTCTI) correction (parameters contained in the LONG_TERM_CTI extension);
- A doubles event energy correction (parameters contained in the COMB_EVT_OFFSET extension);
- A placeholder for a background-dependent gain correction under development (null parameters contained in the NDSCLIN_GAIN extension).

In this document results obtained with different SAS versions and EPN_CTI CCF issues will be compared. For simplicity, "old" refers to the CCF pair EPN_CTI_0031.CCF and EPN_CTI_0032.CCF (used with SAS 13.5), whereas "new" refers to their replacement, EPN_CTI_0045.CCF (used in conjunction with SAS 14.0).

2.1 Energy Dependent LTCTI Correction

The EPIC-pn CTI behaviour is characterised by a secular increase in charge transfer inefficiency (CTI). Event energies are corrected for this through an empirical modelling of the non-LTCTI corrected line centroid trends, obtained from exposures illuminated by the on-board calibration source (*CalClosed* exposures). Details of the method may be found in Smith et al. 2010.

Up to now, a single set of model parameters derived at the Mn-K$_\alpha$ emission line (5.9 keV) was used for the LTCTI correction. However, the LTCTI behaviour is in fact energy dependent, the CTI time dependency in general being stronger at higher energies. The empirical model derived at Mn-K$_\alpha$ therefore yields a non-optimal correction when applied at other energies, and, in particular, at lower energies it results in an energy overcorrection which increases in time.

The latter point is especially pertinent to multi-pixel events such as doubles. Here the issue is compounded, as amplitudes are CTI corrected on an event-wise basis before being merged to obtain the total amplitude. Each of the constituent amplitudes of a multi-pixel event will in general be overcorrected to some extent, leading in time to increasingly incorrect energies, even at Mn-K$_\alpha$ (this is discussed further in section 2.2).

In order to address this, SAS 14.0 together with the new CCF implements an energy dependent LTCTI correction: in addition to the empirical model parameters derived at Mn-K$_\alpha$, the CCF contains a similar parameterisation derived at Al-K$_\alpha$ (1.5 keV). For intermediate energies, the empirical LTCTI correction at a given time is then derived through interpolation in log(E). Event energies < 1.5 keV or > 5.9 keV are corrected with the Al-K$_\alpha$ or Mn-K$_\alpha$ LTCTI model parameters, respectively.

A minor change with respect to the old CCFs is an additional polynomial term in the parameterisation of the LTCTI model time dependency. This allows a sufficiently accurate modelling of the temporal LTCTI behaviour since launch, thus removing the necessity of the epoch-dependent temporal modelling introduced with EPN_CTI_0032.CCF.

The new correction method is illustrated in Fig. 1, which shows, per CCD, the Full Frame mode Al-K$_\alpha$ (top panel) and Mn-K$_\alpha$ (bottom panel) line centroids as determined from non-LTCTI corrected energies. The best fit temporal models from which the values of the LTCTI correction parameters are derived are shown in the solid red lines.

The data used in deriving the parameters are single-pixel events without precursors ("first singles"), which are events for which the energy reconstruction is most accurate. The data are limited to periods of low background, and the spectra have been corrected for out-of-time (OOT) events. Furthermore, in order to optimise the energy reconstruction for targeted sources the data selected for CCD 4 are restricted to an area around the boresight (`RAWY in [181:200]`). For the other CCDs, data from the complete chips are used, although excluding areas with an excessive fraction of OOT events. The spectral fitting includes folding through the detector response, which is especially important for the modelling at Al-K$_\alpha$ due to partial event loss and threshold effects.

As an illustration of the energy dependency of the LTCTI, the Mn-K$_\alpha$ derived LTCTI model, as applied to Al-K$_\alpha$ energies, is shown in the dotted red line in the top panel. The data-to-model

differences indicate the dynamic range of the energy reconstruction discrepancies obtained with the old CCF at Al-K_α.

By construction, the LTCTI correction algorithm assumes a correct energy reconstruction around the time of launch. However, at Al-K_α, for some CCDs the measured line centroids are somewhat below the nominal energy (which is likely due to a detector gain effect and beyond the scope of this document), leading to uncertainties in the LTCTI modelling in the early epoch. It should be noted that this issue is inherent in the LTCTI modelling, and not introduced through the new CCF. In fact, when comparing the old and new LTCTI corrections at Al-K_α it is apparent that the energy dependent LTCTI modelling slightly mitigates the effect.

Similar modelling of Extended Full Frame mode line centroids allows the determination of LTCTI correction parameters for this mode (see Fig. 2).

Large Window, Small Window, Timing and Burst modes are not designed for full-frame illumination, thus complicating the interpretation of *CalClosed* data. As an approximation, for these modes the Full Frame mode parameter values are used.

2.2 Double-Event Energy Correction

Analysis of EPIC-pn imaging mode data has shown a significant difference in reconstructed energy of double events (`PATTERN in [1:4]`) with respect to single-pixel events (`PATTERN == 0`). This difference is characterised by an energy offset, and an additional time dependent component. This is illustrated in Fig. 3 for Mn-K_α. The temporal trend is mainly due to the energy dependence of the LTCTI, as discussed in section 2.1, which, up to the new CCF, has not been accounted for. The energy offset is due to higher order charge loss effects (related essentially to pattern size and circumference) which are not explicitly taken into account in the energy reconstruction.

In order to correct for this, SAS 14.0 introduces an empirical offset correction which is applied to the doubles event energy after merging of the constituent event amplitudes.

The offset values are dependent on read-out mode, pattern orientation and energy. Moreover, there is a detector-wide spatial variation, which in the correction is implemented through a CCD-averaged dependence (the values for CCD 4 are derived from the 20-row region around the boresight). The derived energy offsets are shown in Fig. 4. The energy dependence is determined from a linear interpolation in log(E) using the calibration points at Mn-K_α and Al-K_α. For $E > 5.9$ keV the respective Mn-K_α offset is applied. For $E < 1.5$ keV the applied offset tends asymptotically to zero. Note that the correction is applied to imaging mode data only.

Owing to the approximation of the spatial dependence by a per-CCD dependence, spatial discontinuities in reconstructed double-event energies may affect spectra extracted from multiple CCDs. Caution with interpretation of results is warranted in such cases.

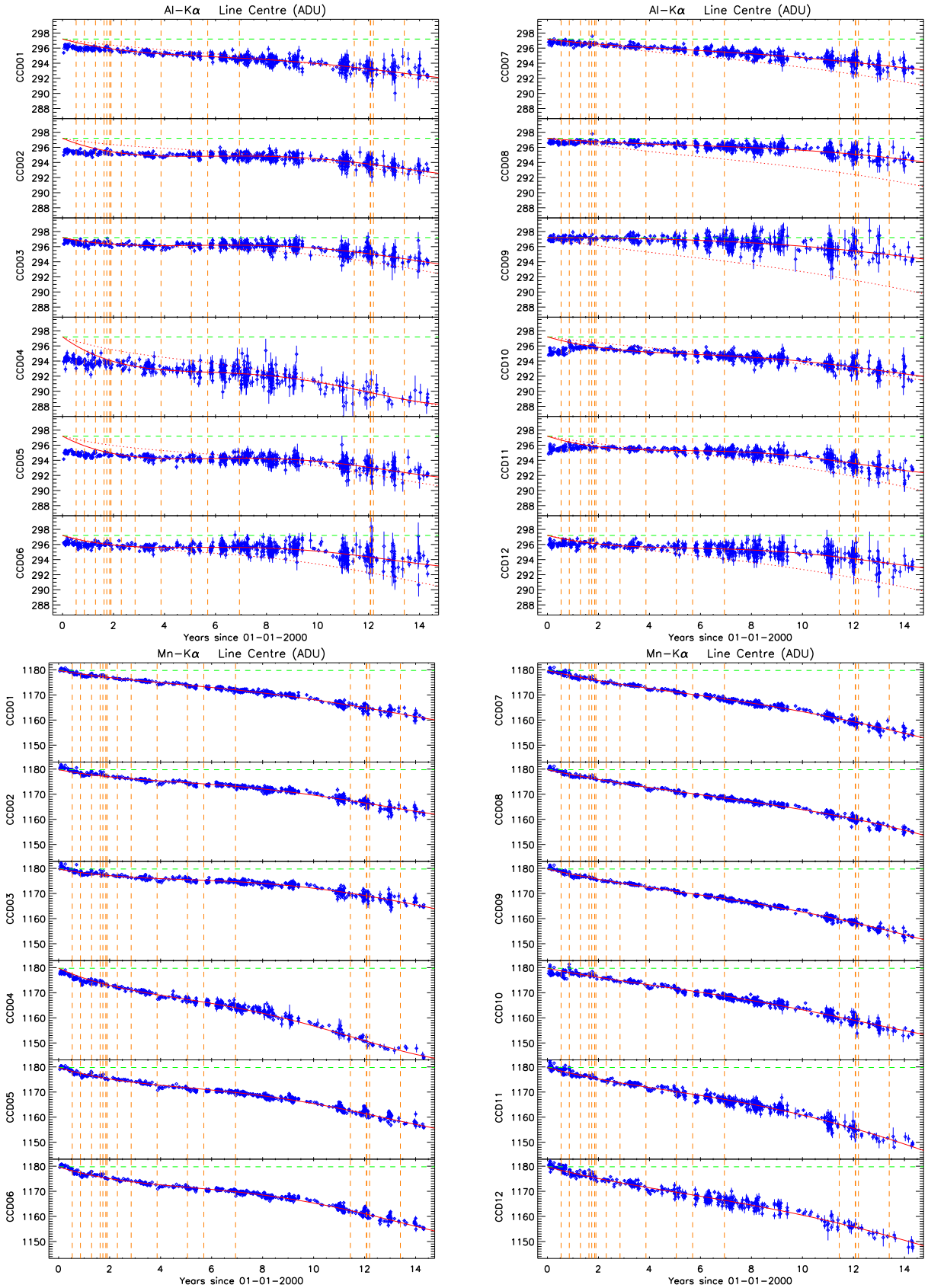

Figure 1: Al-K$_\alpha$ (top) and Mn-K$_\alpha$ (bottom) line centroid energies (in ADU) as determined from Full Frame mode *CalClosed* observations, with no LTCTI correction applied. The data shown here are based on first-single events extracted from the well illuminated areas of the complete CCDs, except for CCD 4, where the data were extracted from a 20-row region around the boresight (for which the CCD 4 model parameters are derived). The horizontal green dashed line shows the nominal line energy, the vertical dashed lines indicate the times of major solar coronal mass ejections. The energy dependent model contained in the new CCF is overlaid in the solid red lines. For comparison, the Mn-K$_\alpha$ model as applied to Al-K$_\alpha$ energies is shown in the dotted red lines in the top panel.

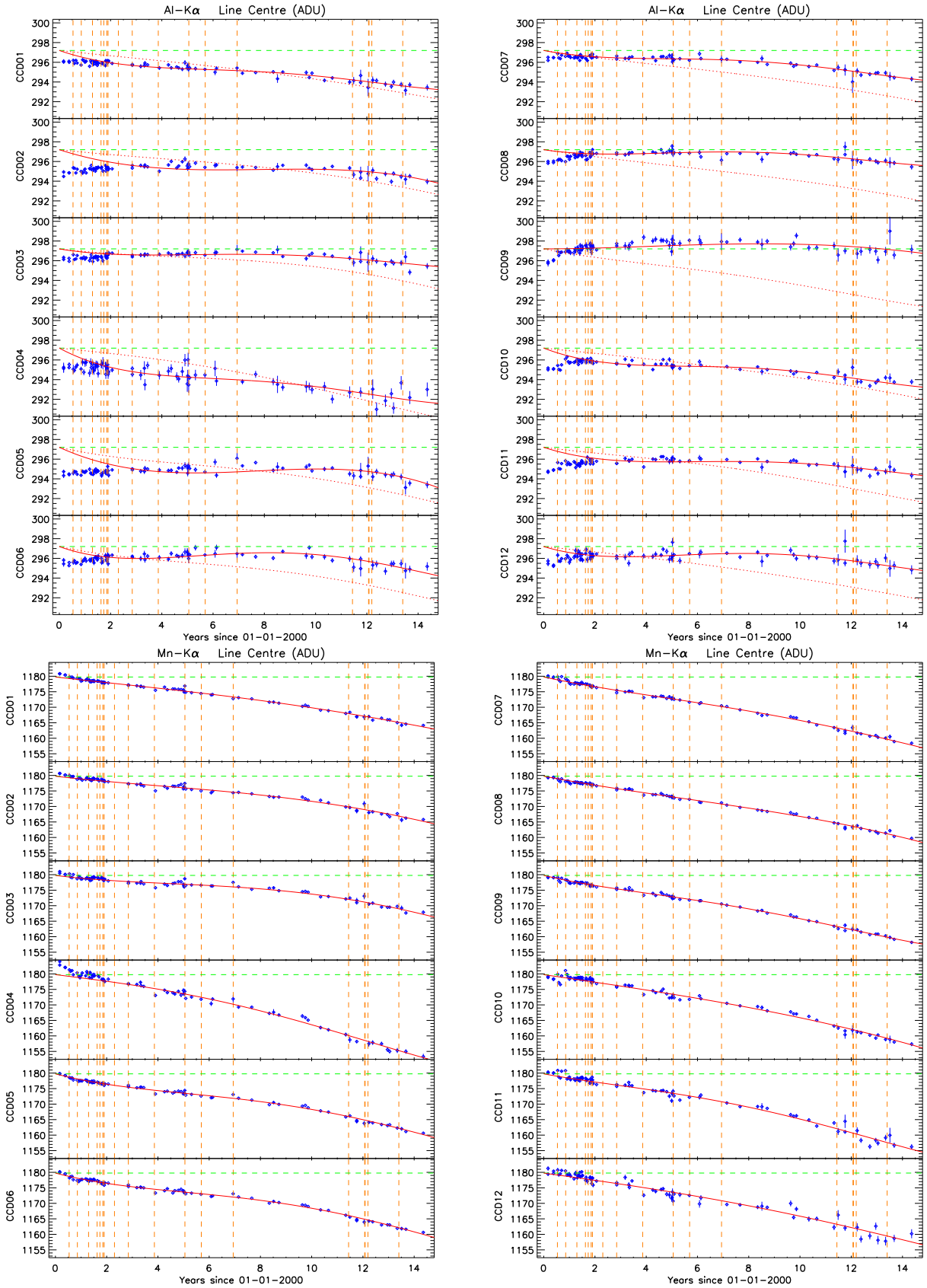

Figure 2: As Fig 1, for Extended Full Frame mode.

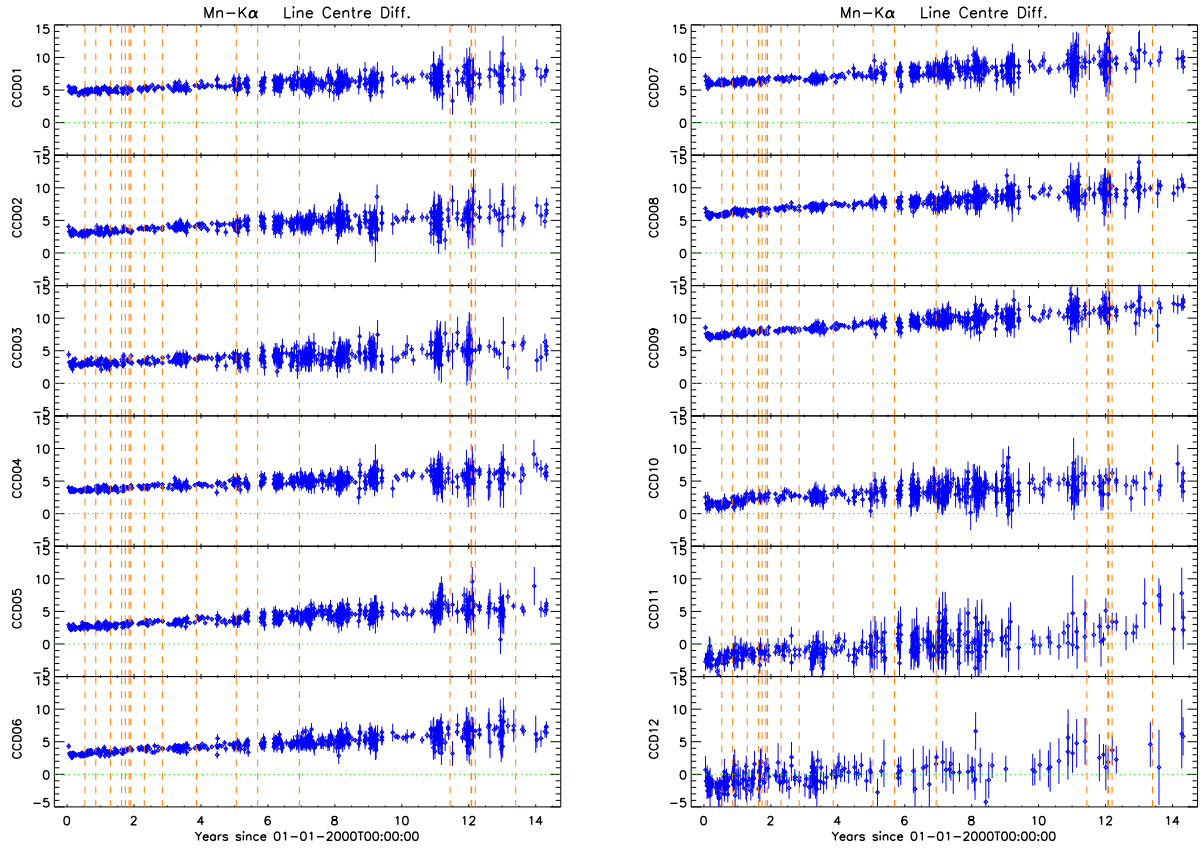

Figure 3: Difference in line centroid energy at Mn-K$_\alpha$ of pattern 1-4 doubles with respect to singles (in ADU), as obtained with SAS 13.5 and the old calibration (results for CCDs 1–6 and CCDs 7–12 shown in the left and right panels, respectively).

2.3 Background-Dependent Gain Correction: Placeholder

A background-dependent gain correction is currently under development. In anticipation of its possible implementation a new NDSCLIN_GAIN extension has been added to the CCF. The parameters contained therein are placeholders and currently result in a null correction. There is consequently no scientific impact related to this change.

3 Scientific Impact and Estimated Quality

3.1 Results from *CalClosed* Data

Several plots detailed in this section are based on the analysis of *CalClosed* data, comparing reconstructed line centroid energies at Al-K$_\alpha$ and Mn-K$_\alpha$ obtained with SAS 13.5 and the old CCFs with those obtained with SAS 14.0 and the new CCF, the latter data having the corrections mentioned

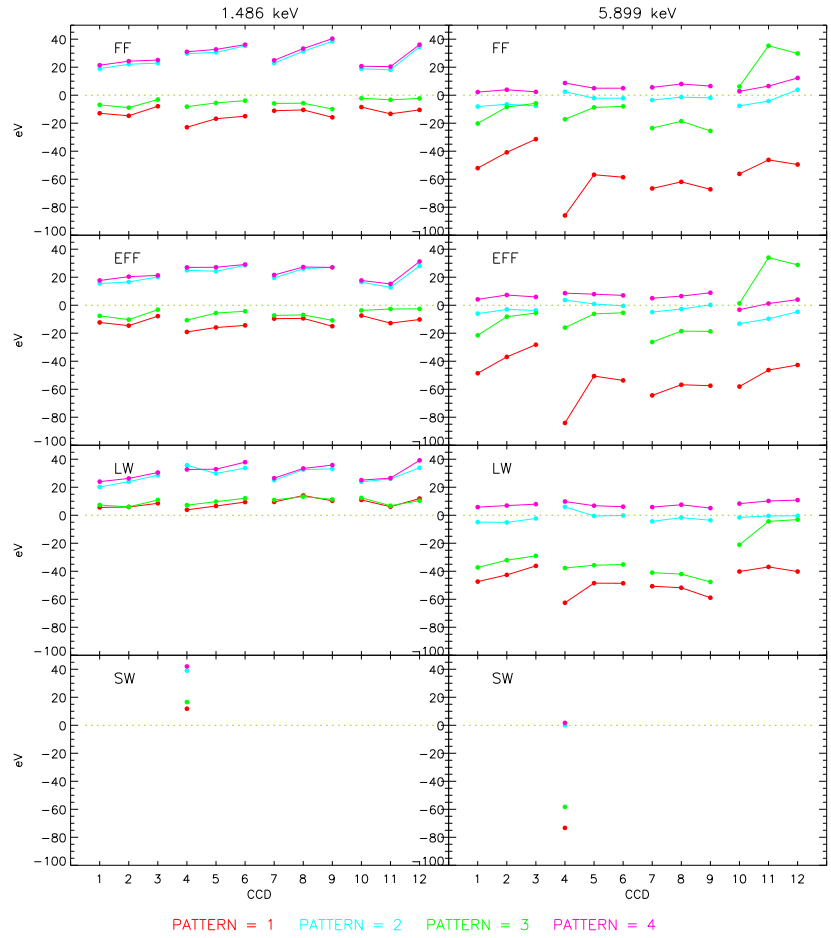

Figure 4: Event energy offsets (in eV) for the empirical doubles-to-singles energy correction. The pattern-type dependent values are colour-coded as indicated. Each panel shows the offset values per CCD (and grouped per quadrant for clarity). Values derived at the Al-K_α and Mn-K_α calibration lines are shown in the left and right columns, respectively. The various imaging modes are ordered row-wise.

in section 2 applied. The figures show the old and new results in the left and right columns, respectively. Data obtained from the complete (well-illuminated) detector area are shown with CCDs 1–6 and CCDs 7–12 in the top and bottom panels, respectively. Additionally, there are plots showing the results obtained with data selected at the boresight location (CCD 4, `RAWY in [181:200]`), for which the CCD 4 modelling has been optimised.

The accuracy obtained with the new calibration of the *CalClosed* energy reconstruction for Full Frame and Extended Full Frame mode data at the boresight is summarised in Table 1. The results are discussed in more detail below.

3.1.1 Single-Pixel Events

Results based on data limited to single-pixel events are unaffected by the doubles offset correction. Hence differences between old and new are solely due to the application of the energy-dependent LTCTI correction.

Mode	Pattern	$\overline{E_{measured} - E_{nominal}}$ (eV)	
		Al-K$_\alpha$ ($E_{nominal} = 1.486$ keV)	Mn-K$_{\alpha_2}$ ($E_{nominal} = 5.888$ keV)
FF	singles	-3 <5> (-2 <3>)	-2 <7> ($+1$ <4>)
	doubles	-6 <7> (-3 <5>)	$+2$ <11> ($+8$ <7>)
EFF	singles	-2 <4> (-1 <3>)	$+2$ <6> ($+1$ <5>)
	doubles	-2 <6> ($+0$ <6>)	$+2$ <6> ($+4$ <5>)

Table 1: Summary of the EPIC-pn energy reconstruction accuracy at the boresight location for *CalClosed* observations taken over the course of the mission. Values shown are the mean and standard deviation (in eV) of the differences between measured line centroid and nominal energy. They are derived from all observations with exposure times ≥ 10 ks since launch; values between parentheses exclude observations taken before 2002.

Full Frame Mode

The reconstructed line centroid energies for Full Frame mode using first-single events extracted from the complete detector area shown in Fig. 5 (Al-K$_\alpha$) and Fig. 6 (Mn-K$_\alpha$); results for data limited to the boresight region are compared in Fig. 9.

As the LTCTI model in the old CCF was derived at Mn-K$_\alpha$, the energy dependence of the LTCTI in the new CCF has negligible impact at this energy. In fact, the essential difference between old and new is due to the additional polynomial term in the temporal modelling: the new CCF yields an energy reconstruction to within the same accuracy as before. Over the course of the mission, for single-pixel data the Mn-K$_\alpha$ reconstructed line energies are in general within ± 12 eV of the nominal value, with typical standard deviation of ~ 4 eV (excluding the badly illuminated CCDs 11 and 12). Larger deviations occur in distinct epochs up to approximately 2001, and in exposures often associated with periods of increased solar activity.

At Al-K$_\alpha$, however, the energy-dependent LTCTI shows an improvement in energy reconstruction, especially from $\sim$ 2002 ($\sim$ revolution 375) onwards. Whereas previously the line centroid showed a continuously increasing trend, the application of the new CCF results in a stable reconstruction to within ± 10 eV of the nominal value (although there remain a few individual exposures with larger deviations). The typical standard deviation in the well illuminated parts of the detector is ~ 3 eV. The energy undercorrection before $\sim$ 2002 is due to the limitations of the LTCTI model and the gain issue mentioned in section 2.1. Nevertheless, with the new CCF the overall dynamic range in energy reconstruction is reduced (or, at worst, remains unchanged).

Extended Full Frame Mode

Similarly, the results for Extended Full Frame mode are shown in Figs. 7 (Al-K$_\alpha$), 8 (Mn-K$_\alpha$) and 10 (boresight data).

As with Full Frame mode data, the main improvement is in the correction of the Al-K$_\alpha$ line energies. Post $\sim$ 2002 the reconstructed energies are stable to within ± 8 eV of the nominal value

($\sim$ 3 eV standard deviation). The Mn-K$_\alpha$ line energies are stable to within $\pm$10 eV, with a typical standard deviation of $\sim$ 4 eV.

3.1.2 Double-Pixel Events

Line centroid energies for Full Frame mode using double-pixel events (i.e. `PATTERN in [1:4]`) extracted from the complete detector area shown in Fig. 11 (Al-K$_\alpha$) and Fig. 12 (Mn-K$_\alpha$); results for data limited to the boresight region are compared in Fig. 15. The equivalent plots for Extended Full Frame mode are Figs. 13, 14 and 16.

Both at Al-K$_\alpha$ and Mn-K$_\alpha$ energies, the old calibration results in a steady temporal increase in doubles energies; the dynamic range is of the order of $\sim$ 25 eV over the course of the mission (there is some CCD dependence). As mentioned in section 2.1, this is due to an increasing overcorrection introduced by the original energy-independent LTCTI model. Application of the energy-dependent LTCTI very much reduces the temporal trend, and effectively removes it for data taken since $\sim$ 2002.

Moreover, at Mn-K$_\alpha$ the old calibration results in a significant overcorrection of double-event energies even at launch (except for CCDs 10–12) by 15–40 eV, depending on CCD. The double-event energy correction significantly reduces these discrepancies.

For Full Frame mode, the new calibration results in a post $\sim$ 2002 doubles energy reconstruction stability to within $\pm$20 eV with a standard deviation of $\sim$ 4 eV at both Al-K$_\alpha$ and Mn-K$_\alpha$. For Extended Full Frame mode the stability is to within $\pm$15 eV with standard deviation of $\sim$ 4 eV.

3.2 Validation on Scientific Data

Scientific validation of the SAS 14.0 and the PN energy scale calibration has been performed using the following sources:

Circinus Galaxy

The Circinus Galaxy is a nearby Seyfert II galaxy which shows a strong Fe-line emission allowing validation of the double-event energy correction upwards of the the Mn-K$_\alpha$ calibration line. It was observed on-axis in Full Frame mode on two occasions: ObsIds 0111240101 and 0701981001. Spectra were extracted for PN single events, PN double events and MOS. PN data were reduced with SAS 13.5 and SAS 14.0 using the old and new calibration, respectively. MOS data were reduced with SAS 13.5 (there are no significant changes to the MOS for SAS 14.0). The emission was fit in the 6.0 – 6.8 keV band with a model consisting of a power-law continuum plus a Gaussian for the Fe-K$_\alpha$ emission at 6.4 keV.

The resulting data and best fit models are shown in the top two rows of Fig. 17 (old and new calibration in left and right panels, respectively). The new calibration yields a clear improvement in

the double event spectra: the original overcorrection (with respect to PN singles and MOS spectra) in Fe-K$_\alpha$ emission line energy has been significantly reduced. This is summarised in Fig 18 (left panel), which shows the resulting Fe-K$_\alpha$ emission line energies. Although the PN single and double-event energies are still not formally consistent, the difference has been reduced from ~ 45 eV to within ~ 15 eV. This is similar, within statistical errors, to the results based on Full Frame mode *CalClosed* data for Mn-K$_\alpha$ at the boresight.

Note that PN single-event spectra are unaffected by the new calibration, which is as expected at energies above Mn-K$_\alpha$.

MCG-5-23-16

The new calibration has further been validated on a Small Window mode observation of the Seyfert I galaxy MCG-5-23-16 (ObsId 0727960201). This source exhibits a strong Fe-K$_\alpha$ emission line, allowing an independent high-energy validation for this mode. Spectra were extracted for PN single events, double events and MOS (annular extraction regions were used to excise the piled-up core), and, as above, PN data were reduced with the old and new calibration. The 5.5 – 7.3 keV band was modelled with a power-law plus Gaussian function.

Best fit results are shown in Fig. 17 (bottom row) and 18 (right panel). The new calibration results in a reduction of PN double events overcorrection from ~ 60 eV down to ~ 20 eV; within statistical errors the PN double events yield consistent results with respect to single events and MOS.

1E 0102.2-7219

The bright SNR 1E 0102.2-7219 has been extensively observed as calibration target over the course of the mission. An empirical model consisting of continuum components and Gaussians for the line emission (Plucinsky et al. 2012), developed in the framework of the International Astronomical Consortium for High Energy Calibration (IACHEC), was used to investigate the impact of the new calibration at low energies (0.55 – 1.36 keV band). PN single-event and double-event spectra for old and new calibration were extracted for 38 observations, and the model line energies of the prominent and isolated O VII, O VIII, Ne IX, Ne X and Mg XI emission lines were left free in order to determine and compare the respective best fit values. The results, in terms of mean measured minus nominal line energies, are shown in Fig. 19.

In comparing double-event spectra in this band it is evident that the new calibration yields energies higher by ~ 10 eV. As all lines except Ne IX were initially undercorrected by a similar amount, they have now been corrected to values consistent with single-event spectra. In the case of O VII and Ne X, the sample standard deviation has also been reduced; this is due to increased temporal stability of the double-event energy reconstruction.

The Ne IX line, in contrast, is now slighty overcorrected for double-event spectra. The reason for this discrepant result is not clear and will require further investigation.

There is no significant impact of the new calibration on single-event spectra in this energy band.

PKS 2155-304 and 3C 273

The impact of the new calibration on flux measurements has been investigated using a sample of 34 observations of the blazars PKS 2155-304 and 3C 273, which have been observed in Small Window mode throughout the mission. Single plus double event (i.e. `PATTERN in [0:4]`) spectra obtained with the old and new calibration were fit with absorbed broken power-law models, and fluxes determined in several spectral bands. Per band, the sample mean flux ratios (new with respect to old calibration) were determined (see Fig 6). The flux differences between old and new calibration are at the level of $\sim 1\%$. The flux increase in the medium energy band can be understood as due to the mitigation of the energy scale undercorrection around Al-K_α, which diminishes towards higher energies. The flux deficit at lower energies is mainly due to the reduced overestimation of the low-energy LTCTI.

4 Test Procedures

Verification of functionality of EPN_CTI_0045.CCF with SAS 14.0: `calview`, `cifbuild`, `epproc`, `epchain`.

5 Expected Updates

As the PN LTCTI will continue to develop in time, model parameters will have to be periodically updated. Inclusion of an extra LTCTI calibration point based on the Cu-K_α fluorescent emission line is under investigation.

6 References

Plucinsky, P.P., et al., 2012, SPIE, 8443, 12

Smith, M.J.S., et al., 2010, XMM-SOC-CAL-SRN-0271
(`http://xmm2.esac.esa.int/docs/documents/CAL-SRN-0271-1-0.ps.gz`)

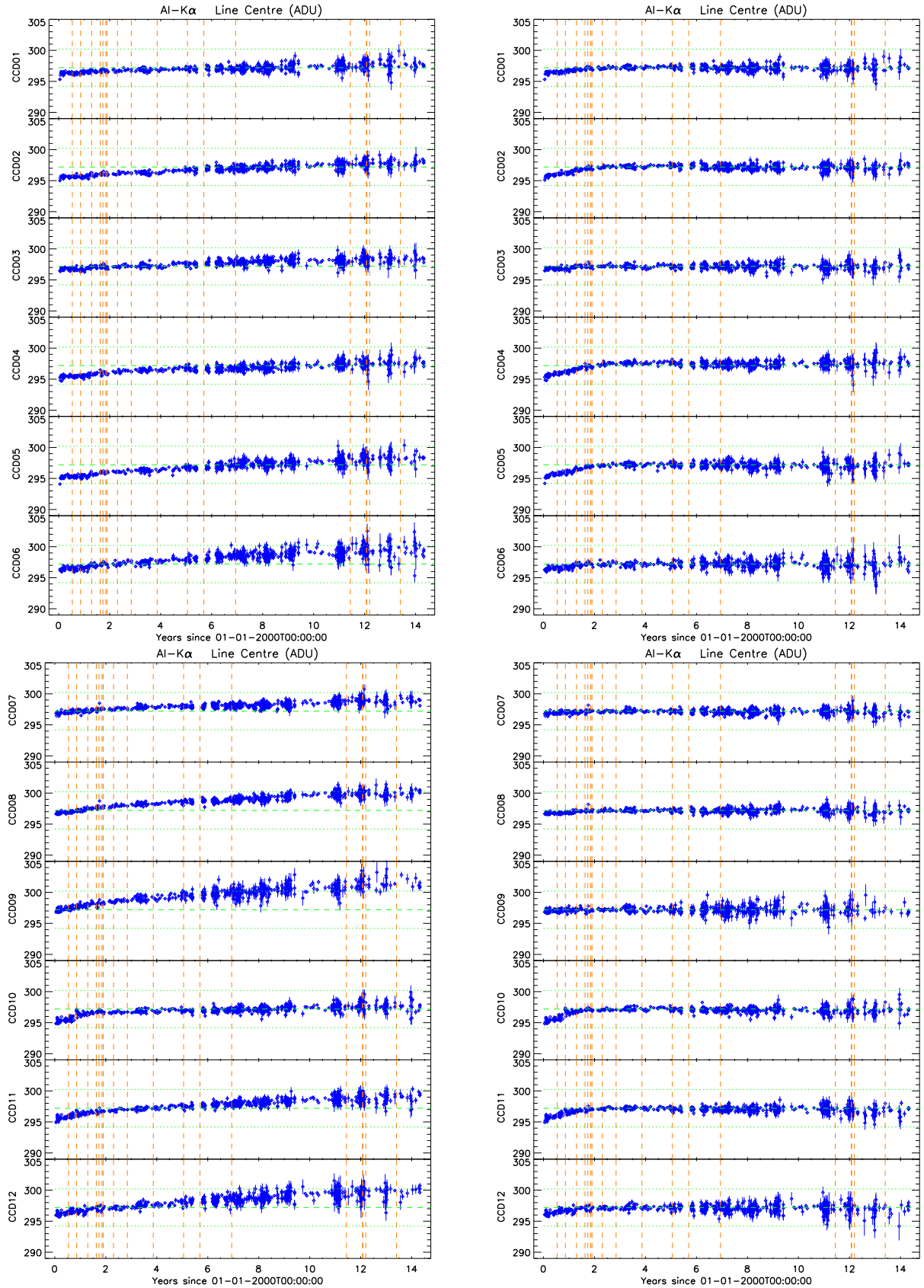

Figure 5: Al-K_α reconstructed line centroid energies (in ADU) as determined from Full Frame mode *CalClosed* observations. Data are based on first-single events extracted from the well illuminated areas of the complete CCDs. Results obtained with the old and new calibration are shown in the left and right columns, respectively. The horizontal green dashed and dotted lines show the nominal line energy and the ±15 eV range. Vertical dashed lines indicate the times of major solar coronal mass ejections.

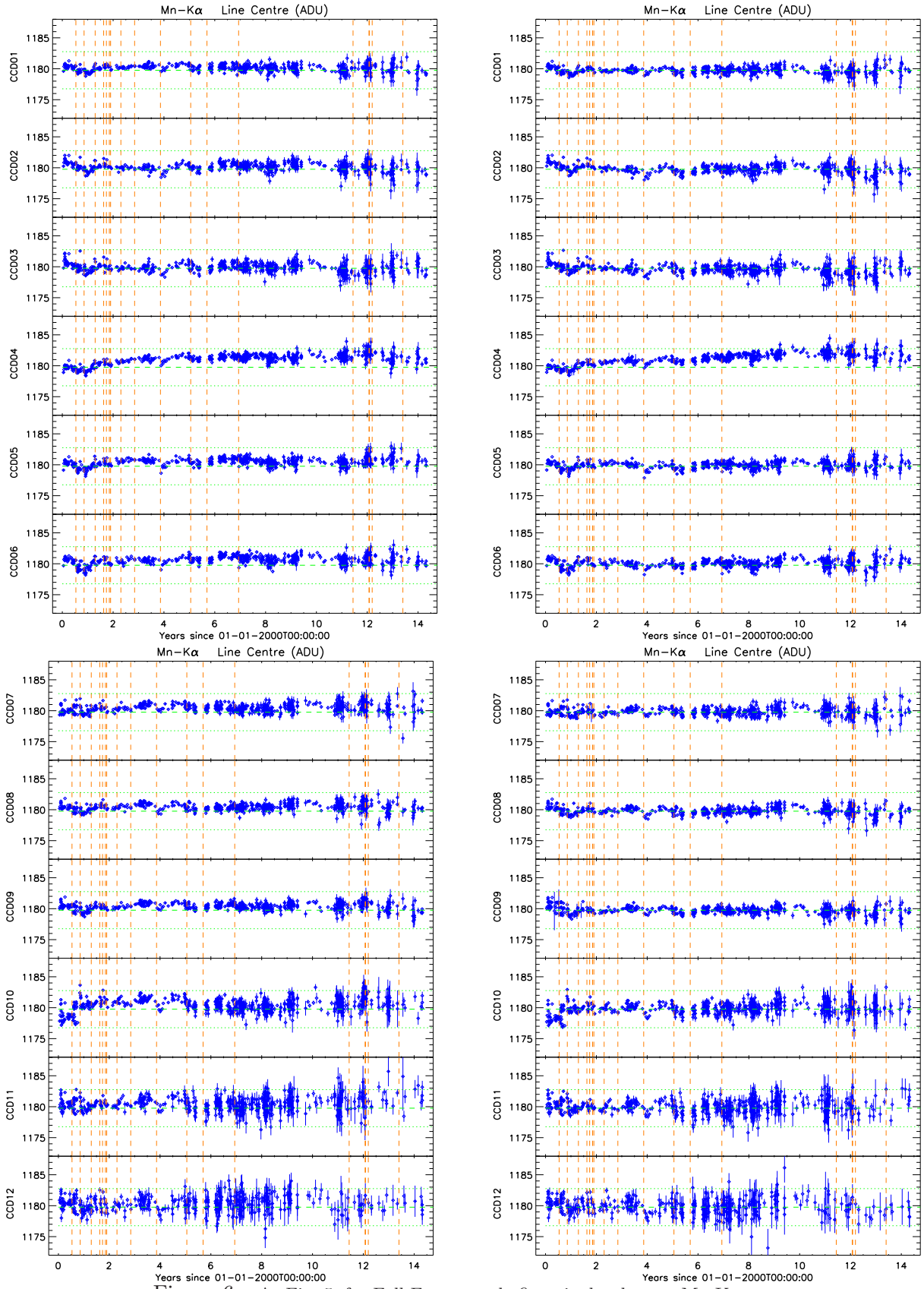

Figure 6: As Fig. 5, for Full Frame mode first-singles data at Mn-K$_\alpha$.

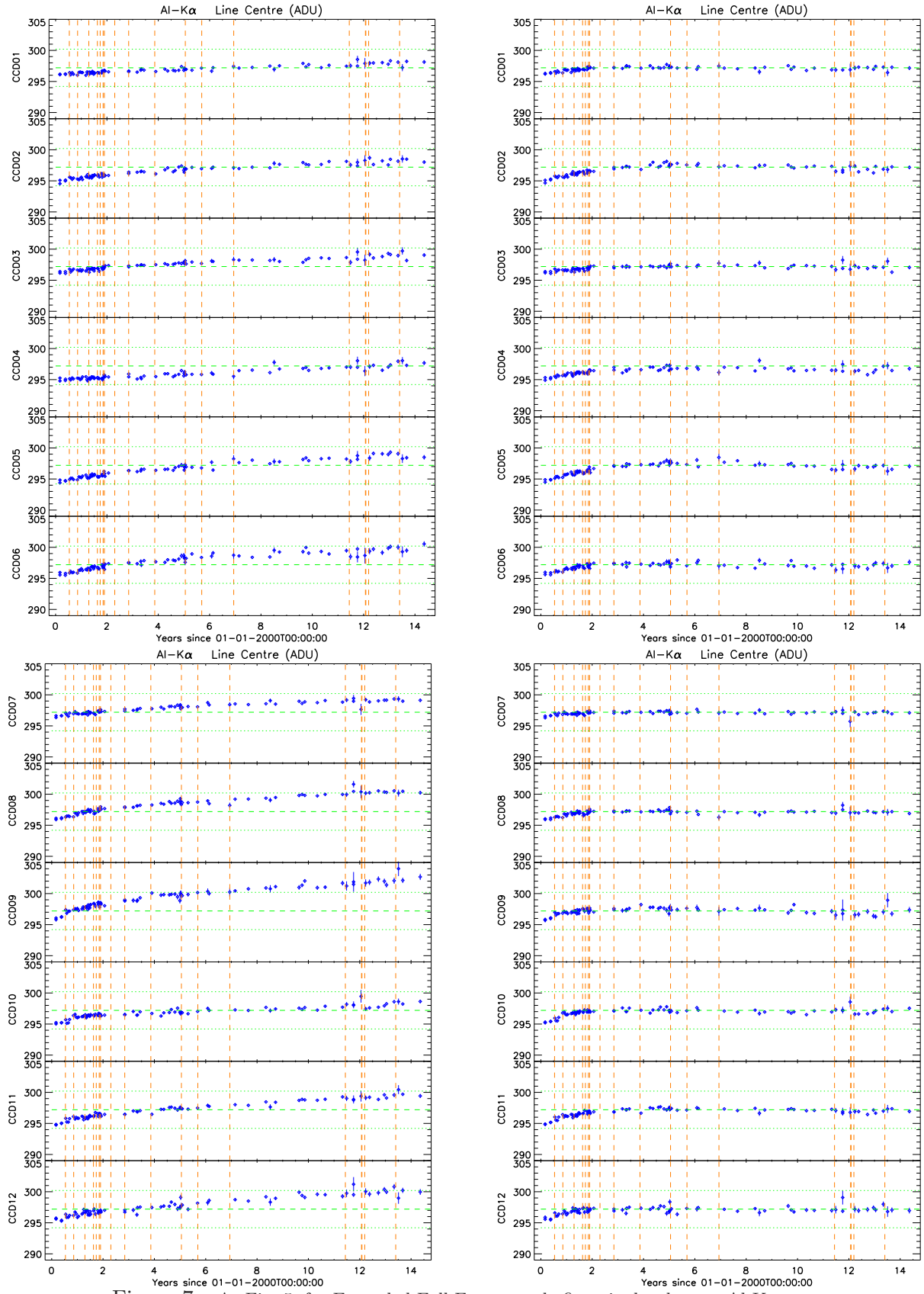

Figure 7: As Fig. 5, for Extended Full Frame mode first-singles data at Al-K_α.

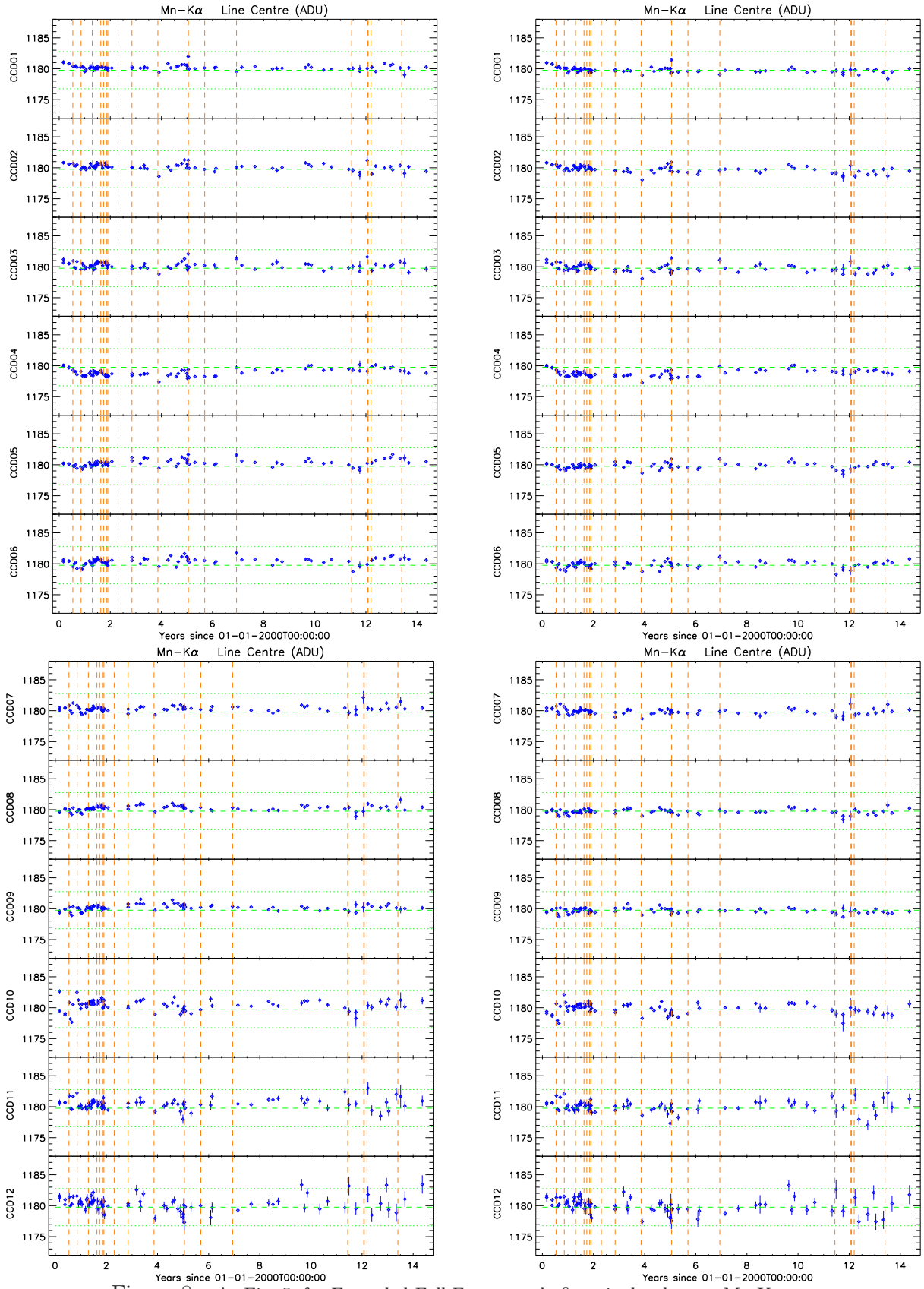

Figure 8: As Fig. 5, for Extended Full Frame mode first-singles data at Mn-K$_\alpha$.

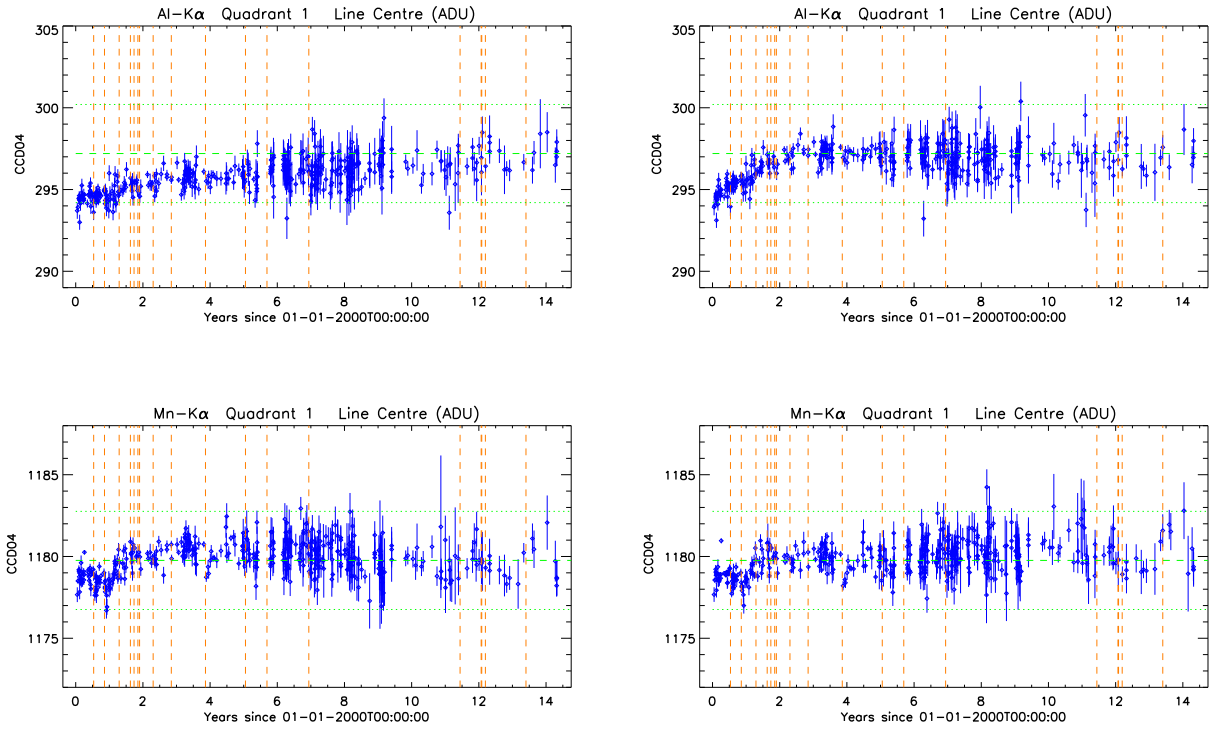

Figure 9: As Fig. 5, however for Full Frame mode first-singles data restricted to the CCD 4 boresight area. As before, left and right columns show the old and new calibration results, respectively. Al-K$_\alpha$ data are shown in the top panels and Mn-K$_\alpha$ data in the bottom panels.

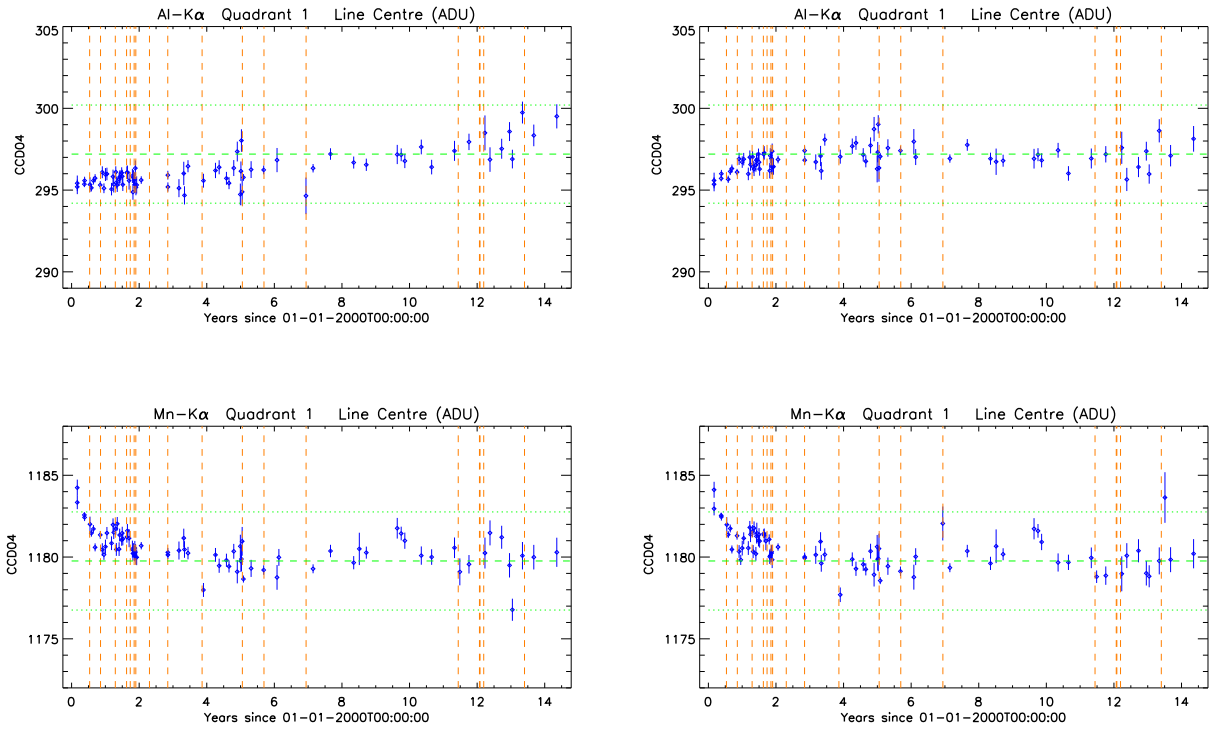

Figure 10: As Fig 9, for Extended Full Frame mode first-singles data taken at the boresight region.

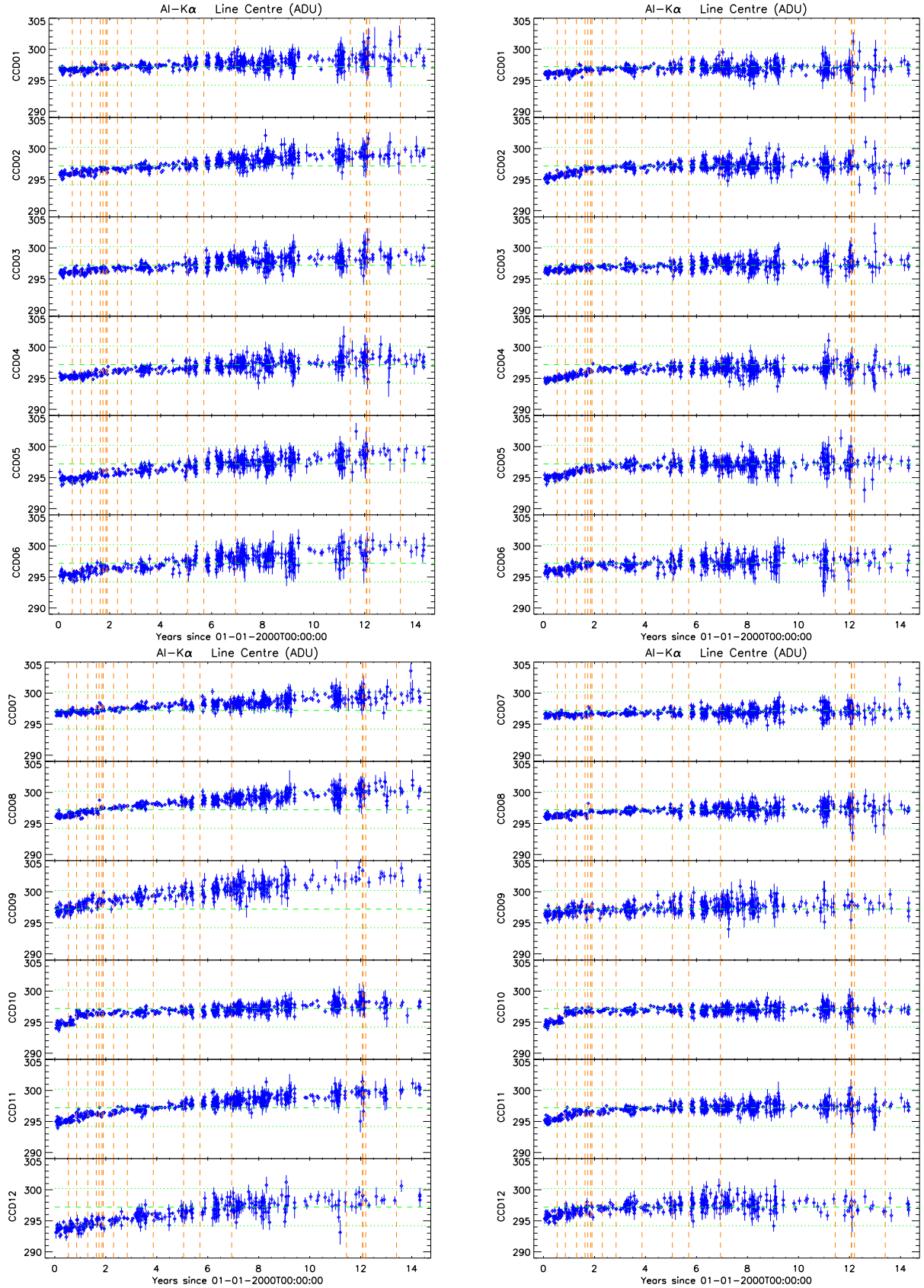

Figure 11: Al-K$_\alpha$ reconstructed line centroid energies (in ADU) as determined from Full Frame mode *CalClosed* observations. Data are based on double-pixel events extracted from the well illuminated areas of the complete CCDs. Results obtained with the old and new calibration are shown in the left and right columns, respectively.

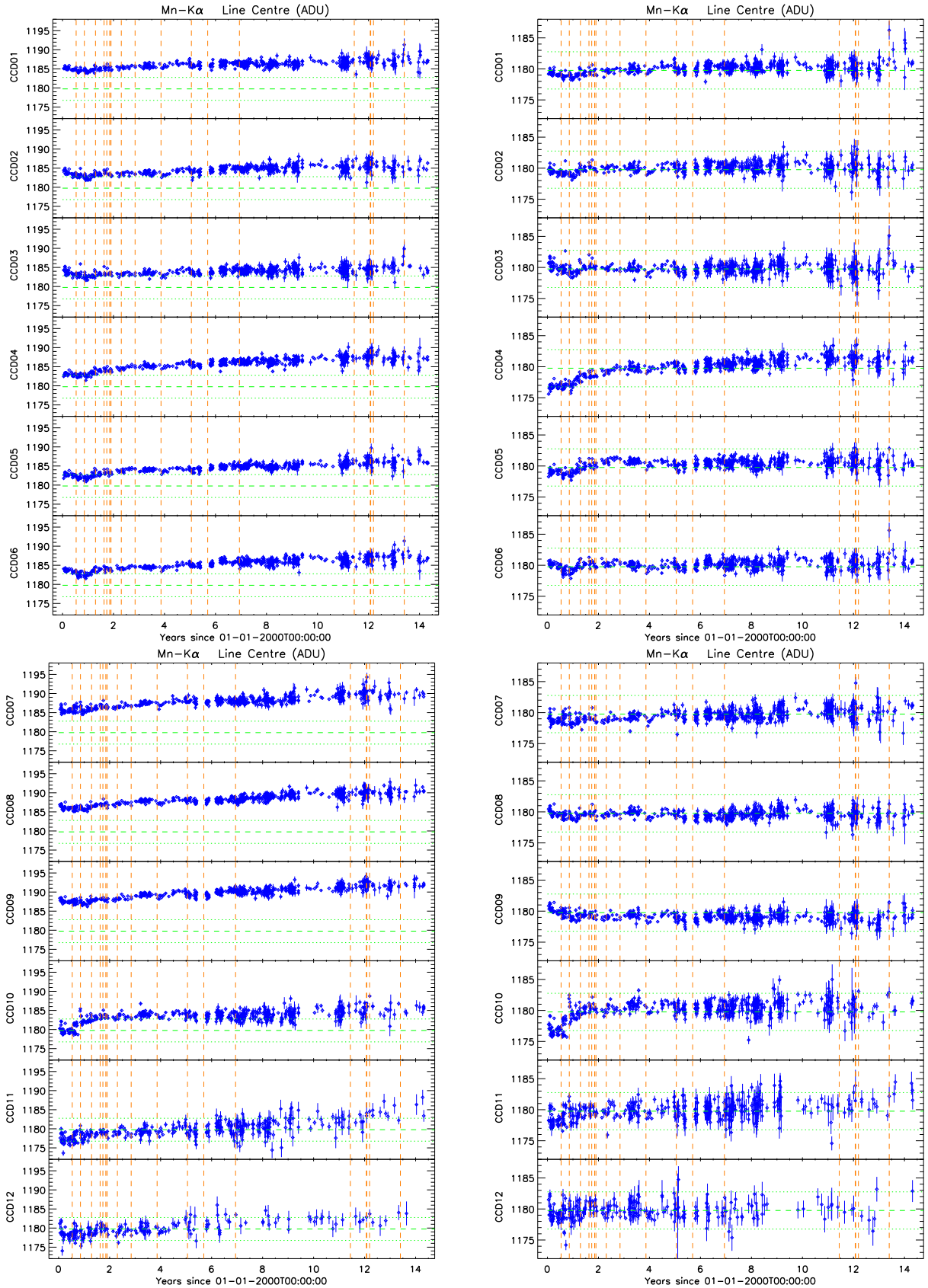

Figure 12: As Fig. 11, for Full Frame mode double-pixel events at Mn-K$_\alpha$. Note that the left panels are plotted with an increased y-axis dynamic range.

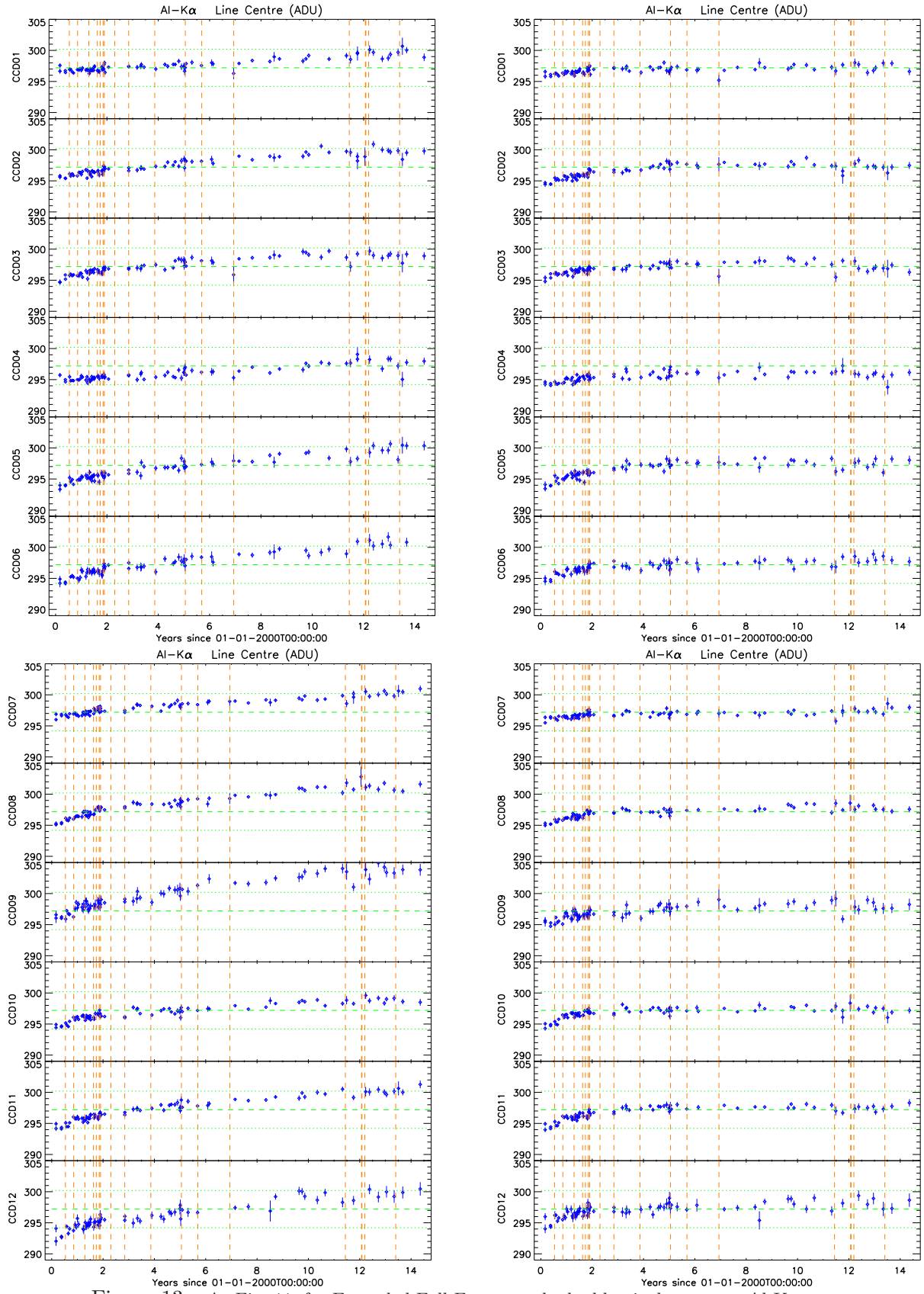

Figure 13: As Fig. 11, for Extended Full Frame mode double-pixel events at Al-K_α.

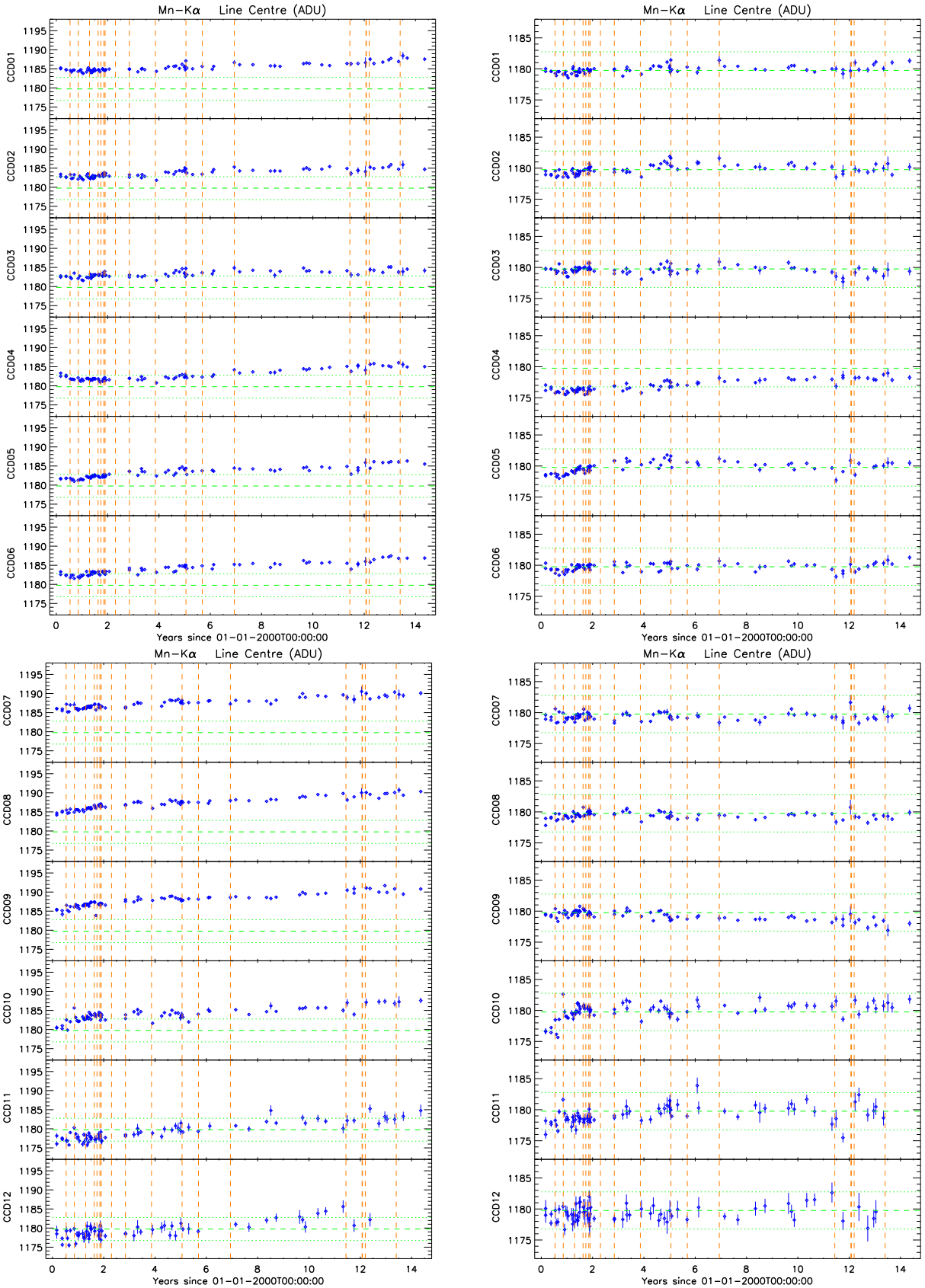

Figure 14: As Fig. 11, for Extended Full Frame mode double-pixel events at Mn-K$_\alpha$. Left panels are plotted with a larger y-axis dynamic range.

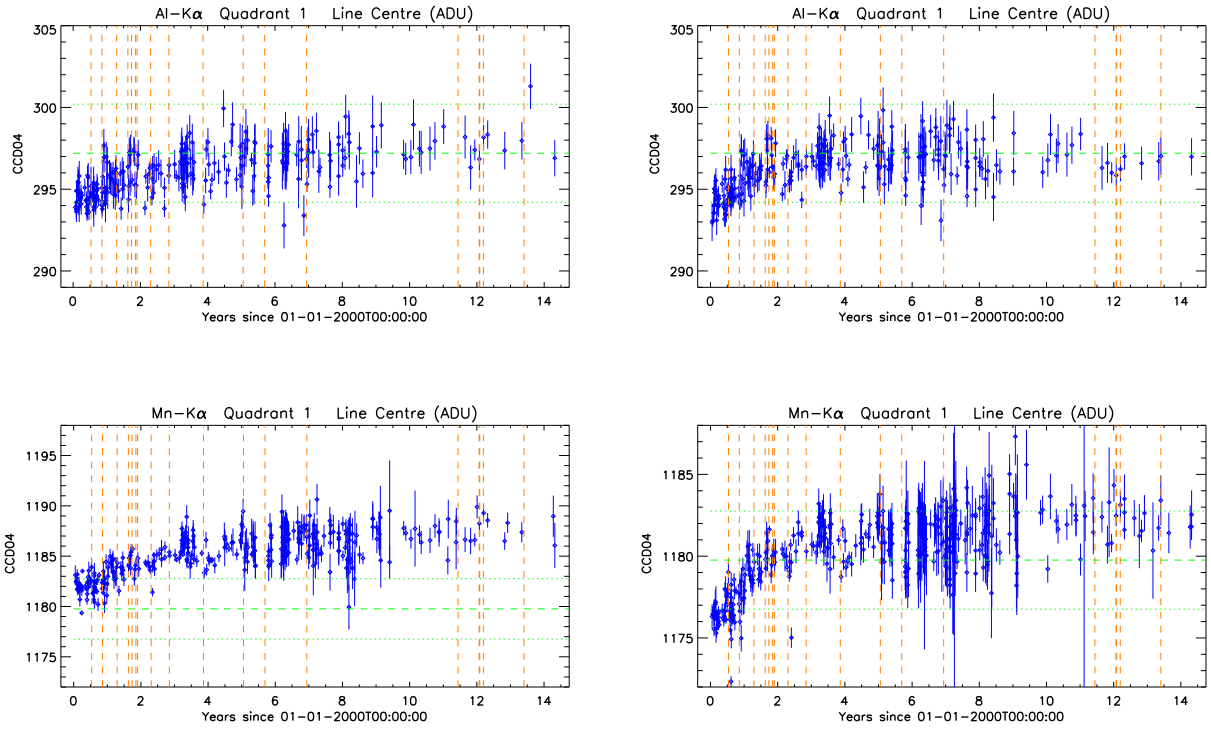

Figure 15: As Fig. 11, however for Full Frame mode double-pixel events restricted to the CCD 4 boresight area. As before, left and right columns show the old and new calibration results, respectively. Al-K$_\alpha$ data are shown in the top panels and Mn-K$_\alpha$ data in the bottom panels (the latter are plotted with differing y-axis dynamic ranges.)

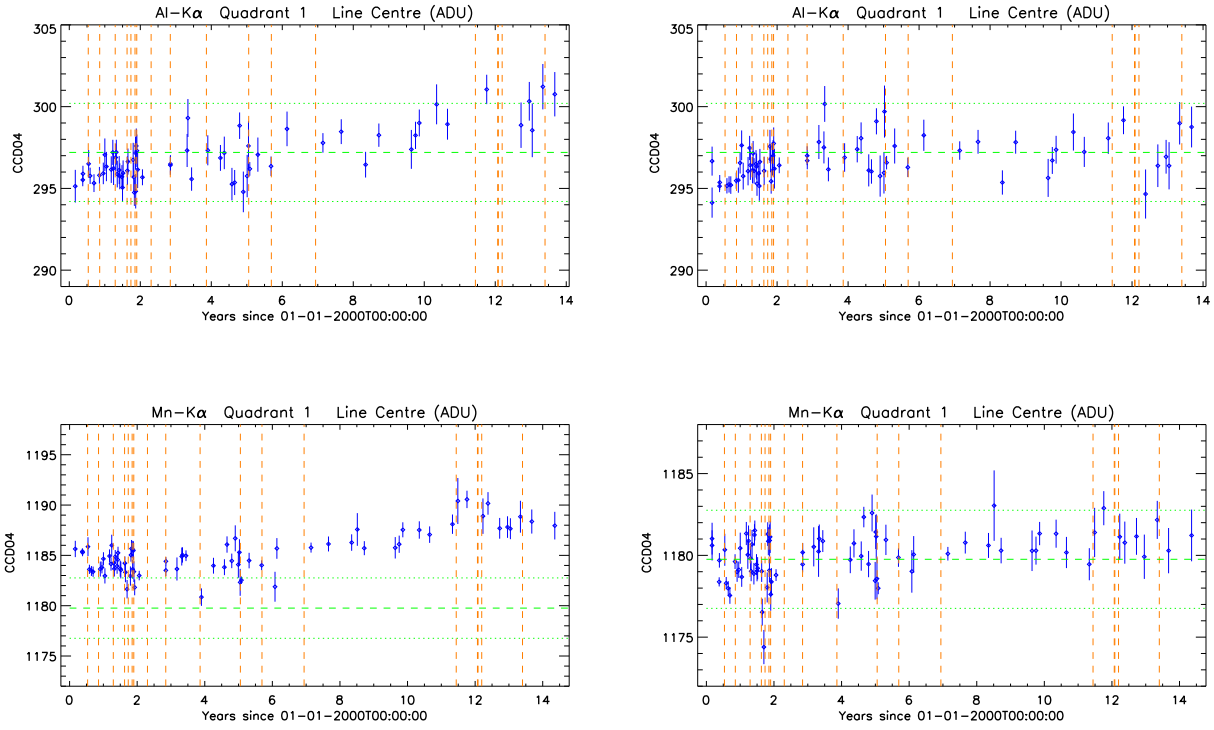

Figure 16: As Fig 15, for Extended Full Frame mode double-pixel events taken at the boresight region.

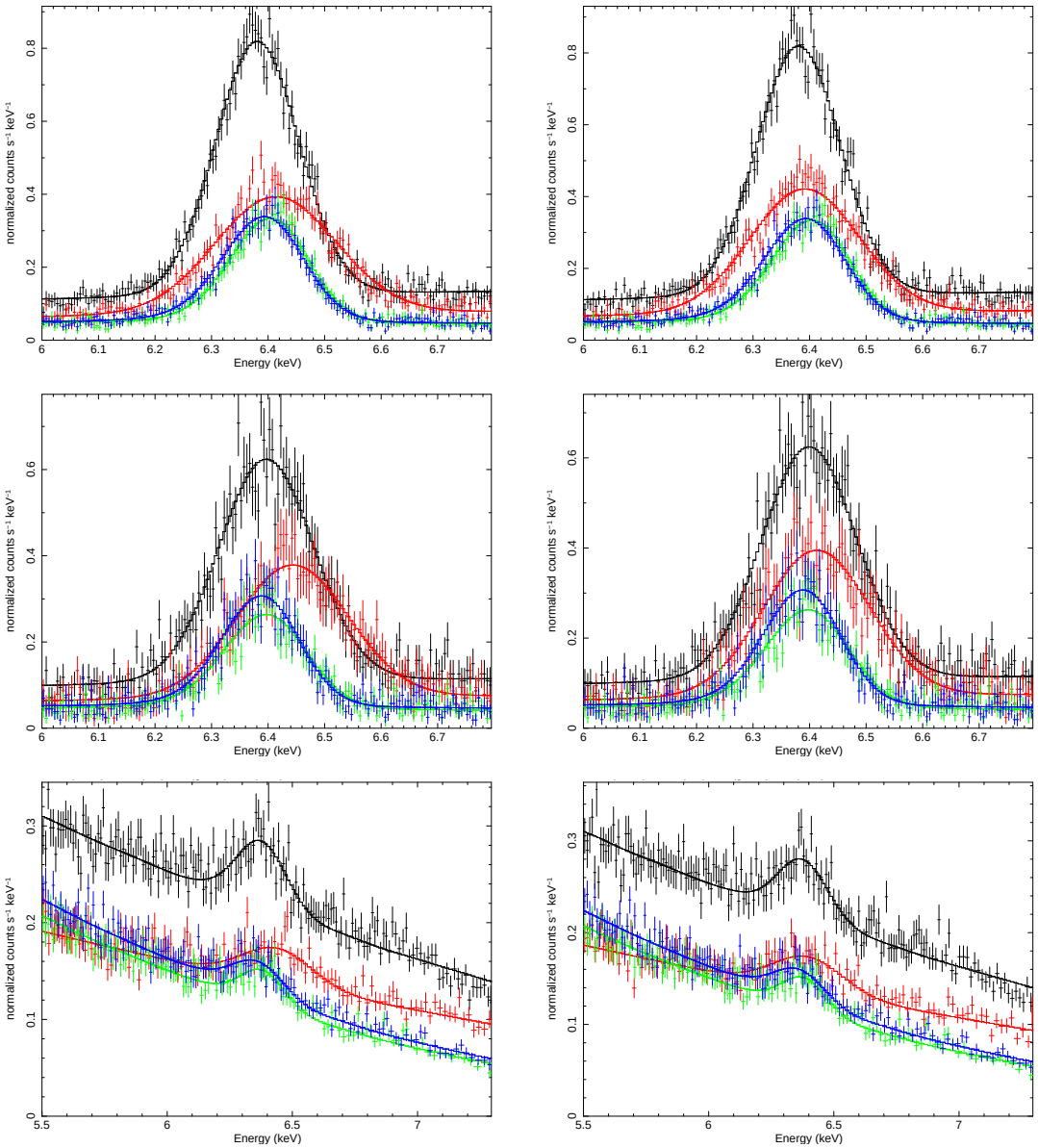

Figure 17: Data and best fits to a continuum plus Gaussian model of the Fe-K$_\alpha$ emission for two observations of Circinus Galaxy in FF mode (top two rows, from top to bottom obsids 0111240101 and 0701981001) and one observation of MCG-5-23-16 in SW mode (bottom row, obsid 0727960201). Each plot contains the following EPIC spectra: PN single-pixel events (black), PN double-pixel events (red), MOS1 (green) and MOS2 (blue). The MOS data were reduced with SAS 13.5. PN data reduced with SAS 13.5 and using old EPN_CTI CCFs are shown in the left column. PN data reduced with SAS 14.0 and using the new EPN_CTI_0045.CCF are shown in the right column. The MOS data were reduced with SAS 13.5 (the MOS spectra do not significantly change with SAS 14.0).

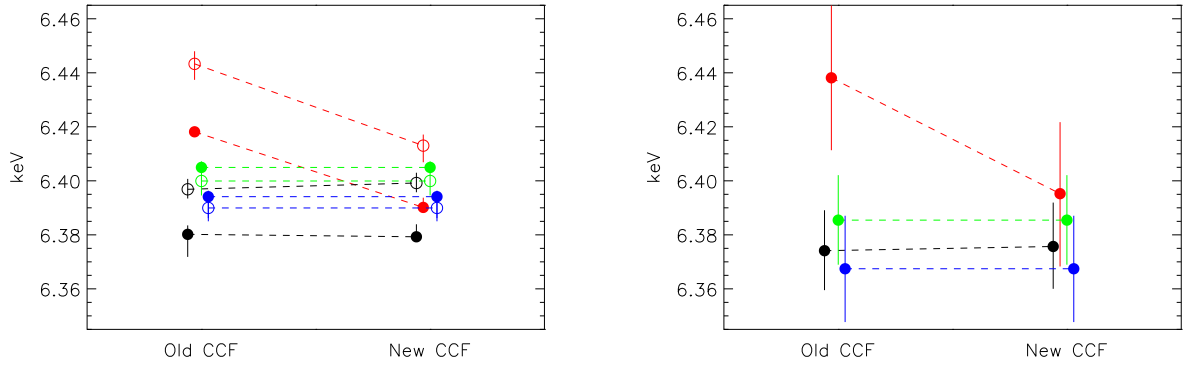

Figure 18: Fe-K$_\alpha$ line centroid energies comparing old and new calibration: Circinus Galaxy (left panel; closed circles: ObsId 0111240101, open circles: ObsId 0701981001) and MCG-5-23-16 (right panel). The colour coding as in Fig. 17.

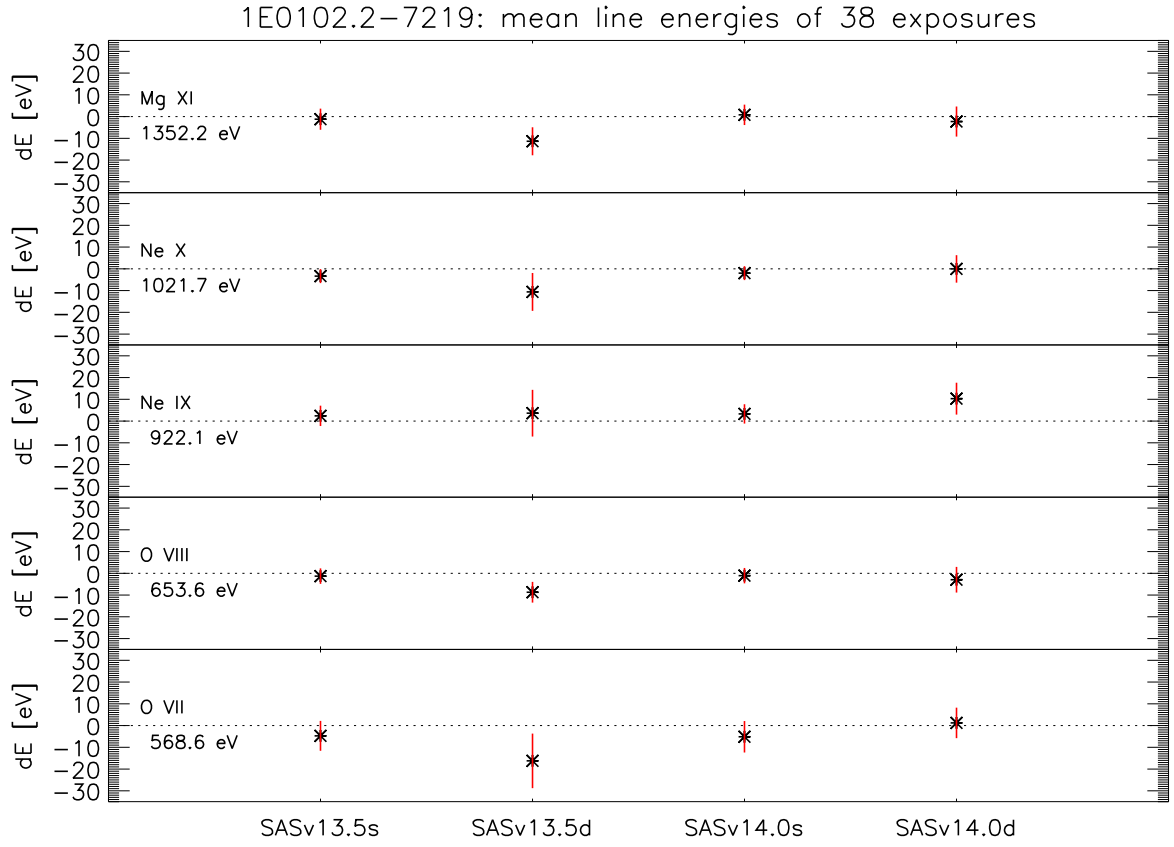

Figure 19: Results of an analysis of emission line energies as determined by PN from a sample of 38 observations of the SNR 1E 0102.2-7219. The panels show the following lines (from top to bottom): Mg XI, Ne X, Ne IX, O VIII and O VII. Energies are expressed in terms of the mean difference (in eV) between measured value and nominal energy; the errors show the standard deviation. The PN data and reduction used are ordered column-wise (from left to right): SAS 13.5 single events, SAS 13.5 double events, SAS 14.0 single events, SAS 14.0 double events.

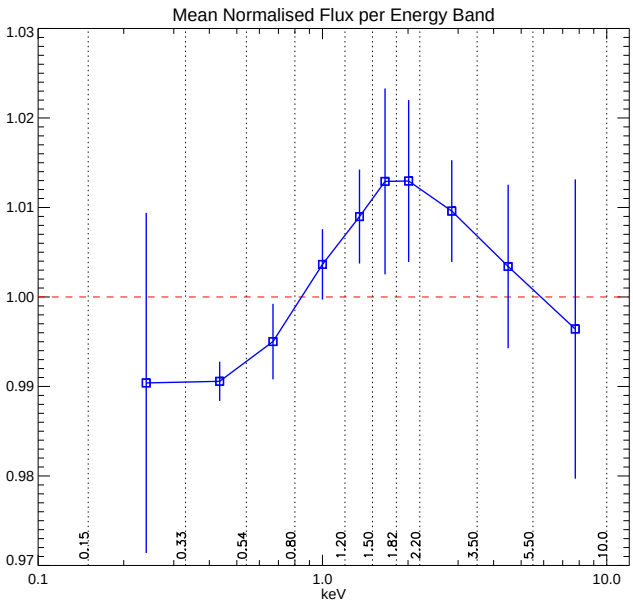

Figure 20: Comparison of spectral band fluxes based on a sample of blazar observations (PKS 2155-304 and 3C 273). Spectra were extracted using single plus double events. The data points show the sample mean flux ratios (new with respect to old calibration) in several energy bands. Error bars denote the sample standard deviation.